Journal of the Korean Physical Society, , pp. 0∼0

Physical Model of the C_{bc} for the Linearity Characteristics of AlGaAs/GaAs HBTs

Woonyun Kim, Sanghoon Kang, Kyungho Lee, Minchul Chung, Youngoo Yang, and Bumman Kim*

Department of Electronic and Electrical Engineering, and Microwave Application Research Center, Pohang University of Science and Technology, Pohang, Kyungbuk 790-784

(Received Date Month Year, in final from Date Month Year)

It is well-known that C_{bc} is the dominant nonlinear element in HBTs. To study its behavior, we have developed an analytical nonlinear HBT equivalent circuit model. The present model includes the effect of the ionized donor charge in the depleted collector region being compensated for by the injected mobile charge. The model-based simulation shows that, at a small signal range, the IM3 of the normal HBT has the normal 3 : 1 gain slope generated by the nonlinearity of C_{bc}. At a large signal level, the load line passes through some regions with constant C_{bc} because its collector is fully depleted by the injected free carriers, and the growth rate of IM3 is decreased. The punch-through collector HBT has constant C_{bc} during the whole RF cycle, and the IM3, which is generated by g_m nonlinearity, has the normal 3 : 1 gain slope for all input signal levels. Therefore, the IM3 level is significantly lower for the punch-through HBT at a low power level, but the IM3s of both devices are comparable at a high power level. The experiment supports our proposed model.

I. INTRODUCTION

The transmitters of the handsets of digital mobile communication systems require highly efficient linear power amplifiers [1–4]. Heterojunction bipolar transistors (HBTs) are widely used for the amplifiers, and their intermodulation (IM) behavior has been extensively measured and analyzed [4–12]. It is commonly known that C_{bc} is the dominant nonlinear source and should be linearized to reduce intermodulation distortions [7,9–12]. HBTs with punch-through collectors at the operation bias point show a higher third-order intermoduation intercept point (IP3) than normal HBTs. However, the IP3 represents a small signal behavior only. To investigate the contribution of the nonlinear C_{bc} to the distortion at a large signal level, we developed an analytical nonlinear HBT model for a commercially available harmonic balance simulator, ADS, using symbolically defined devices (SDDs). By considering self-heating and recombination effects, the model accurately describes the bias dependence of the current gain. The physically based large-signal HBT model includes the effect of the ionized donor charge in the depleted collector region, which is compensated for by the injected mobile charge. C_{bc} is, therefore, dependent not only on the base-collector voltage but also on the collector current.

In order to study the effects of C_{bc} on the nonlinear properties, we compared two kinds of HBTs. A punch-through HBT has a collector that is fully depleted by the collector bias voltage even at low current levels. It has a constant C_{bc} during the whole RF cycle, and its third-order intermodulation (IM3) has the normal 3 : 1 gain slope for all signal levels. On the other hand, an HBT with a normal collector exhibits a strongly nonlinear C_{bc} at small input powers, and the IP3 of the HBT is a lot lower than that of the punch-through HBT. At large signal levels, however, the collector can be fully depleted by the injected charge and C_{bc} becomes constant for some portion of RF cycle. Therefore, the gain slope of IM3 is decreased, and at very high power levels, IM3 is almost comparable to that of the punch-through HBT. To verify the model, we fabricated and tested HBTs with punch-through collectors and normal collectors. The experimental data support the results of the present model.

II. NONLINEAR HBT MODEL

The device model parameters used in the simulation are summarized in Table 1. All equivalent circuit parameter values were obtained as functions of the HBT structures [13,14]. Figure 1 shows the nonlinear equivalent circuit for the analysis. In the figure, R_e, R_{b1}, and R_{b2} are linear components while R_c, I_{ee}, I_{cc}, C_{be}, C_{bci}, and C_{bcx} are bias-dependent nonlinear components. They are calculated from the HBT structure. L_e, L_b, L_c, C_{pbc}, C_{pce}, and C_{pbe} are parasitics and are extracted by

*Tel:+82-54-279-2231, Fax: +82-54-279-2903
E-mail: bmkim@postech.ac.kr

Table 1. HBT model parameters used in the simulation.

Symbol	Value	Symbol	Value
ρ_{EC}	$1 \times 10^{-6}\ \Omega cm^2$	$\epsilon_{E,AlGaAs}$	$1.09 \times 10^{-12}\ F/cm$
ρ_{BC}	$3 \times 10^{-6}\ \Omega cm^2$	ϵ_B, ϵ_C	$1.16 \times 10^{-12}\ F/cm$
ρ_{CC}	$1 \times 10^{-6}\ \Omega cm^2$	V_{TH}	0.0259 V
L_E	22 μm	ΔE_C	0.205 ev
L_B	26 μm	ΔE_V	0.109 eV
L_C	26 μm	N_{CD}	$4.7 \times 10^{17}\ cm^{-3}$
S_E	2 μm	N_{VA}	$7.0 \times 10^{18}\ cm^{-3}$
S_B	1 μm	m_n^*	$0.07m_o$
S_C	3 μm	m_p^*	$0.5m_o$
S_{EB}	0.2 μm	v_{sat}	$4.1 \times 10^7\ cm/s$
S_{BC}	3 μm	J_{ER}	$5 \times 10^{-14}\ A/cm^2$
S_{CD}	4 μm	m	1.92
L_e	50 pH	C_{pbe}	0.11 fF
L_b	0.47 pH	C_{pce}	0.10 fF
L_c	0.29 pH	C_{pbc}	9.4 fF

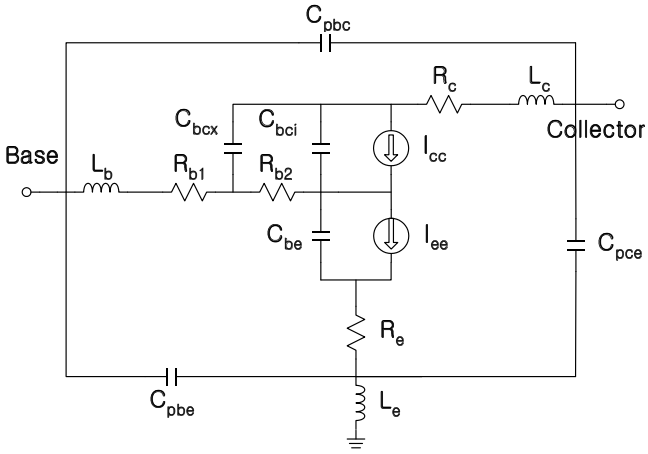

Figure 1. HBT large-signal model.

fitting the measured s-parameter data. The parasitics for our devices are also listed in Table 1.

C_{bci}, the intrinsic base-collector capacitance, is carefully modelled. The model includes the effect of the ionized donor charge in the depleted collector region, which was compensated by the injected mobile charge. The depletion thickness (X_C) in the collector is modulated by the injection charges [15], and even for the device with an undepleted collector at a given collector bias, the collector can be fully depleted by the charge. Assuming that the conduction current in the collector region is mostly due to drift and the carriers travel at a constant velocity of v_{sat}, the mobile carrier concentration in the base-collector junction is simply $n = J_C/qv_{sat}$, where J_C is the collector current density. The Poisson equation in the depleted collector region simplifies to

$$\frac{d\varepsilon}{dx} = \frac{1}{\epsilon_s}(qN_C - \frac{J_C}{v_{sat}}). \tag{1}$$

By integration of both sides over the depletion region from x=0 to X_C with the boundary condition of electric field, $\varepsilon(X_C) = 0$, we obtain

$$\varepsilon(x) = \frac{1}{\epsilon_s}(qN_C - \frac{J_C}{v_{sat}})(x - X_C). \tag{2}$$

We obtain the potential by integrating one more time from x=0 to X_C:

$$V_{cbj} + \phi_{cb} = \frac{1}{\epsilon_s}(qN_C - \frac{J_C}{v_{sat}})\frac{{X_C}^2}{2}. \tag{3}$$

Here, ϕ_{cb} represents the built-in potential. The junction voltage is equal to the applied base-collector bias (V_{cb}) minus the resistive voltage drop in the undepleted collector layer:

$$V_{cbj} = V_{cb} - J_C\rho_C(W_C - X_C), \tag{4}$$

where ρ_C is the resistivity of the undepleted collector layer. The depletion thickness, X_C, depends on J_C and V_{BC} and is given by

$$X_C = \frac{\epsilon_s\rho_C J_C}{qN_C}(1 - \frac{J_C}{J_1})^{-1} + \sqrt{(\frac{\epsilon_s\rho_C J_C}{qN_C})^2(1 - \frac{J_C}{J_1})^{-2} + \frac{2\epsilon(V_{cb} + \phi_{bi})}{qN_C}(1 - \frac{J_C}{J_1})^{-1} - \frac{2\epsilon_s\rho_C J_C W_C}{qN_C}(1 - \frac{J_C}{J_1})^{-1}}, \tag{5}$$

where $J_1 = qv_{sat}N_C$. This equation is applicable for a collector current density J_C smaller than J_1. The charge at the intrinsic region of the base-collector junction, Q_{bci}, is given by

$$Q_{bci} = A_E X_C(qN_C - \frac{J_C}{v_{sat}}). \tag{6}$$

Therefore, C_{bci} depends not only on the base-collector voltage but also on the collector current. The intrinsic base-collector capacitor, C_{bci}, is obtained from the $\frac{dQ_{bci}}{dV_{bc}}$ routine of ADS. The current dependence of C_{bci} at the bias voltage, $V_{CE} = 3.5$ V, is extracted from the model and is depicted in Figure 2. The C_{bci} of the punch-through HBT is constant for all collector-current levels. The C_{bci} of a normal HBT depends, however, on the collector-current density. As the collector current increases, the depleted region thickens, and C_{bci} becomes

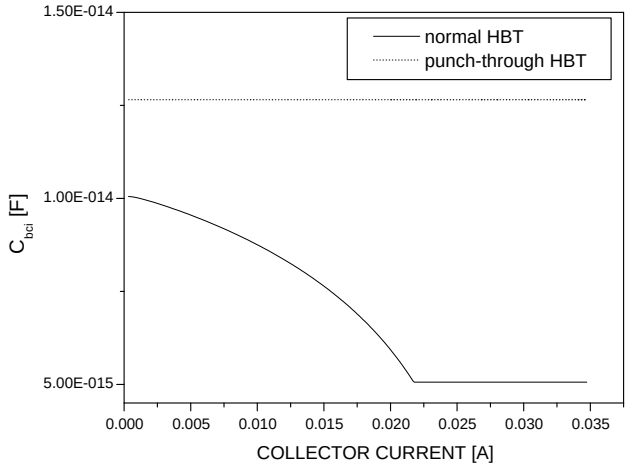

Figure 2. Collector current dependency of C_{bci} at V_{CE} = 3.5 V for a normal HBT and a punch-through HBT.

smaller. At a higher current density (above 28 kA/cm^2), the collector is fully depleted, and C_{bci} becomes constant.

It can be assumed that the injected electrons seldom enter the extrinsic collector area [15]. The compensation effects by the mobile charge are negligible in the extrinsic collector region. The depletion thickness (X_{CX}) in the extrinsic region and the extrinsic base-collector capacitance C_{bcx} are modeled as

$$X_{CX} = \sqrt{\frac{2\epsilon_s(\phi_{bi}+V_{cb})}{qN_C}}, \quad (7)$$

$$C_{bcx} = \frac{\epsilon_s(A_C-A_E)}{X_{CX}}, for X_{CX} \le W_C$$
$$= \frac{\epsilon_s(A_C-A_E)}{W_C}, for X_{CX} > W_C. \quad (8)$$

A detailed description of the other model parameters was reported previously [10]. Self-heating effects are also considered [16]. The Kirk current density of a GaAs-based HBT is much higher than that of a Si BJTs [17–19], and the base push out is not observed within the bias range of our measurement.

III. EXPERIMENTAL AND THEORETICAL RESULTS

We fabricated AlGaAs/GaAs HBT's using the self-aligned base metal (SABM) process with mesa isolation. The AlGaAs/GaAs HBT epi-structure grown by MOCVD consists of an n^+-InGaAs cap layer, an n-GaAs layer, an n-AlGaAs emitter layer, a C-doped p^+-GaAs base layer, an n-GaAs collector layer, and an n^+-GaAs sub-collector layer. The HBTs with punch-through collectors and normal collectors have the same structures except for their collector thicknesses. The HBT with the punch-through structure has a 0.4-μm-thick collector doped to $2 \times 10^{16} cm^{-3}$ and the other has a 1.0-μm-thick collector with the same doping. A thick gold metal layer is deposited on the emitter to improve the electrical and the thermal performances. We also use the emitter widening process using polyimide. The substrate is lapped to a thickness of 100 μm and emitter is grounded by via hole.

The maximum current gains of both HBTs are about 30. The breakdown voltage at an open base, BV_{ceo}, is 10 V for the punch-through collector and 17 V for the normal one. The f_T and f_{max} are 70 GHz and 80 GHz, respectively, at I_C=18 mA and V_{CE}=2.0 V for the punch-through collector structure and 55 GHz and 125 GHz, respectively, at I_C=16 mA and V_{CE}=2.3 V for the normal collector structure.

The power test results at 2 GHz for the 32-emitter-finger HBTs are illustrated in Figure 3, together with the two-tone test results. The DC bias point is I_C=350 mA and V_{CE}=3.5 V. The punch-through HBT and the normal HBT exhibit power gains of 16.6 dB and 16.9 dB, with output powers of 28.9 dBm and 28.6 dBm and power added efficiency (P.A.E.) of 51% and 59%, respectively, at 1-dB gain compression point. The source and the load pulls using an automatic tuner are performed to locate the matching points for maximum gain and output power. Input matching impedances for the punch-through device and the normal device are 5.24-j1.05 and 4.74-j1.51, respectively. The output matching impedances are 6.33-j2.70 and 5.61-j7.87, respectively.

A two-tone test is carried out at 2 GHz. The two-tone spacing is 1 MHz to reduce the thermal effects on the linearity of AlGaAs/GaAs [20]. The matching points and the bias conditions for the two HBTs are the same as they are for the power test. Their third-order IM distortion behaviors are remarkably different, as seen in the Figure 3. At low input powers, the HBT with the punch-through collector has a much lower IM3 than the normal HBT. The IP3 difference is 14.8 dB (39.5 dBm vs. 24.7 dBm). As the input power level increases (above -8.26 dBm in our case), the IM3 of the normal HBT grows at a much slower pace than the normal 3 : 1 slope. However, at large input powers, the slope increases at a ratio larger than 3 : 1, and in this region, the IMD3 for both HBTs are comparable.

To understand the IM3 behaviors of the two HBTs, we performed harmonic balance simulations at 2 GHz for both HBT structures with 32 finger emitter. The operation conditions, bias points, and matching impedances were set at the same values as for the measurement case. Figure 4 shows the simulation results, and a reasonable agreement is seen between the measured and simulated data. Our model indicates that the IM3 of the punch-through HBT is generated by the g_m nonlinearity since the collector is fully depleted and C_{bci} is constant for all power levels. IM3 follows the 3 : 1 gain slope reasonably well. The origin of the different IM3 characteristics of the

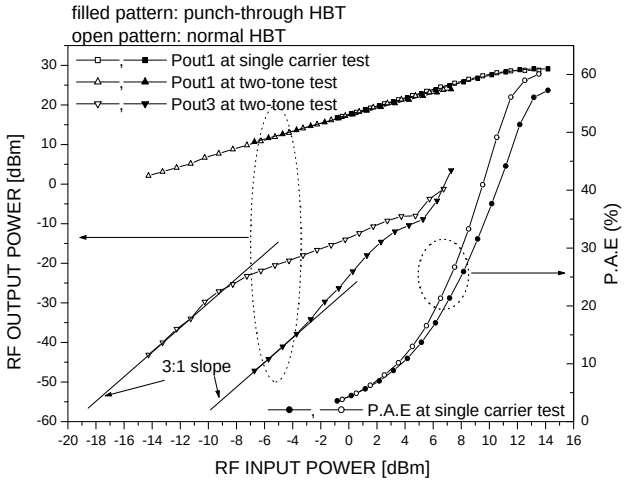

Figure 3. Single-tone and two-tone test results for the fabricated power HBTs.

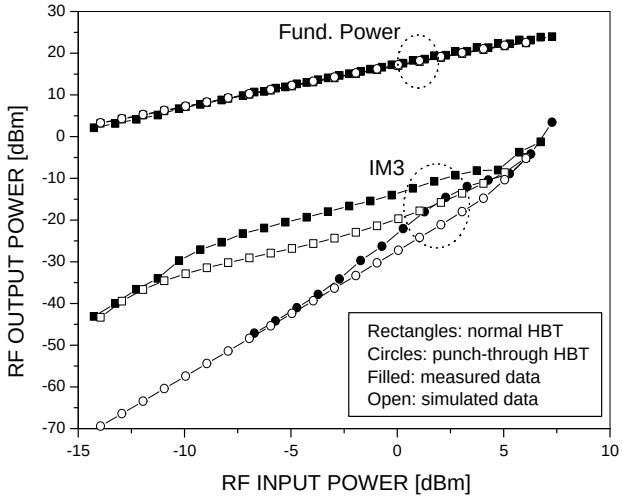

Figure 4. Simulation results of the output power and its IM3 for 32-finger HBTs. For comparison, the measured data are also included.

two HBTs is C_{bci} since our physical models are exactly identical (except for the C_{bci} of the charge-modulated collector depletion layer). For the normal HBT, the IM can have a normal $3:1$ gain slope at small signals because the load line moves in the region near to the bias point and sees the nonlinearity of C_{bci}. For large signal levels, the load line passes through some region with constant C_{bci} formed by the fully depleted collector, and the growth rate of IM3 is decreased.

IV. CONCLUSION

The collector capacitance of HBT is the dominant nonlinear element, and the HBT with punch-though collector is reported to have improved linear characteristics. To study the C_{bc} effect on the linearity, we compared the properties of HBTs with a punch-through collector and a normal collector. For that purpose, we developed an analytical nonlinear HBT equivalent circuit model. The present model includes the effect of the ionized charge in the depleted collector region, which is compensated for by the injected mobile charge. For the normal HBT, the IM can have a normal $3:1$ gain slope in the small-signal range because the load line moves in the region near to the bias point and sees the nonlinearity of C_{bci}. For large signal levels, the load line passes through some region with constant C_{bci}, which is formed by the fully depleted collector, and the growth rate of IM3 is decreased. The punch-through HBT has a constant C_{bci} during the whole RF cycle, and its IM3 has the normal $3:1$ gain slope for all input signal levels. Therefore, the IM3 level is lower for the punch-through collector HBT at lower power levels, but the IM3 of both devices are comparable at high power levels. To verify our simulation results, HBTs with punch-through collectors and normal collectors were fabricated and tested. At a low input signal, the HBT with the punch-through collector has a much lower IM3 than the normal HBT has. The IP3 difference is 14.8 dB (39.5 dBm vs. 24.7 dBm). The differences are reduced as the power level is increased, and around P_{1dB}, the IM3 level of the two HBTs are quite comparable.

ACKNOWLEDGMENTS

This work was supported in part by the Agency for Defense Development and in part by the Brain Korea 21 Project of the Ministry of Education. The authors would like to thank H. C. Seo, Eoncom Ltd., for his assistance with the sawing process. They also wish to thank B. Ihn and D. S. Pang, Samsung Electronics Co., for their help with the lapping process.

REFERENCES

[1] Christopher T. M. Chang and Han-Tzong Yuan, *Proc. IEEE,* **81(12)**, 1727 (1993).

[2] P. M. Asbeck, M. F. Chang, J. J. Corcoran, J. F. Jensen, R. N. Nottenburg, A. Oki, and H. T. Yuan, *IEEE GaAs IC Symp. Tech. Dig.,* Monterey, CA., pp. 7-10, Oct. 1991.

[3] Guang-Bo Gao, David J. Roulston, and Hadis Morkoc, *IEEE Trans. Electron Dev.* **ED-37(5)**, 1199 (1990).

[4] M. E. Kim, A. K. Oki, J. B. Camou, P. D. Chow, B. L. Nelson, D. M. Smith, J. C. Canyon, C. C. Yang, R. Dixit, and B. R. Allen, *IEEE GaAs IC Symposium Digest,* pp. 117-120, Nov. 1988.

[5] Stephen A. Maas, Bradford L. Nelson, and Donald L. Tait, *IEEE Trans. Microwave Theory and Tech.,* **MTT-40(3)**, 442 (1992).

[6] Taisuke Iwai, Shiro Ohara, Horoshi Yamada, Yasuhiro Yamaguchi, Kenji Imanishi, and Kazukiyo Joshin, *IEEE Trans. Electron Devices,* **ED-45(6)**, 1196 (1998).
[7] K. W. Kobayashi, J. C. Cowles, L. T. Tran, A. Gutierrez-Aitken, M. Nishimoto, J. H. Elliott, T. R. Block, A. K. Oki, and D. C. Streit, *IEEE Solid-State Circ."* **34(9)**, 1188 (1999).
[8] Apostolos Samelis and Dimitris Pavlidis, *IEEE Trans. Microwave Theory and Tech.,* **MTT-40(12)** 2374 (1992)
[9] Nan Lei Wang, Wu Jing Ho, and J. A. Higgins, *IEEE Trans. Microwave Theory and Tech.,* **MTT-42(10)**, 1845 (1994).
[10] Joonwoo Lee, Woonyun Kim, Taemoon Rho, and Bumman Kim, *IEEE Trans. Microwave Theory and Tech.,* **MTT-45(12)**, 2065 (1997).
[11] Peter Asbeck, *IEEE MTT-S Int. Microwave Symp. Workshop,* Baltimore, Maryland, June 1998.
[12] M. Iwamoto, T. S. Low, C. P. Hutchinson, J. B. Scott, A. Cognata, X. Qin, L. H. Camnitz, P. M. Asbeck, and D. C. D'Avanzo, *IEEE MTT-S Int. Microwave Symp. Dig.,* Boston, MA, pp. 757-760, Jun. 2000.
[13] H. C. Casey, Jr., and M. B. Panish, *Heterostructure Lasers,* (Academic, New York, 1978).
[14] A. A. Grinberg, M. S. Shur, R. J. Fischer, and H. Morkoc, *IEEE Trans. Electron Dev.* **ED-31(12)**, 1758 (1984).
[15] William Liu, *Handbook of III-V Heterojunction Bipolar Transistor,* (Wiley, New York, 1998).
[16] J. J. Liou, L. L. Liou, C. I. Huang, and B. Bayraktaroglu, *IEEE Trans. Electron Dev.* **ED-40(9)**, 1570 (1993).
[17] C. T. Kirk, Jr., *IRE Trans. Electron Dev.* **9**, 164 (1962).
[18] P. C. Chris Grossman, and J. Chroma, Jr., *IEEE Trans. on Microwave Theory and Tech.* **MTT-40(3)**, 449 (1992).
[19] Joonwoo Lee, Bumman Kim, Youngsik Kim, and Sungsoo Park, *Solid-State Electronics* **37(8)**, 1485 (1994).
[20] K. Lu, P. M. McIntosh, C. M. Snowden, and P. D. Pollard, *IEEE MTT-S Int. Microwave Symp. Dig.,* San Francisco, CA., pp. 1373-1376, June 1996.